RESIDENCE TIME CONTROL IN MICROMIXERS WITH VORTEX SHEDDING

Shigang Zhang, Manish K Tiwari *
Nanoengineered Systems Lab, UCL Mechanical Engineering, University College London, London, WC1E 7JE
m.tiwari@ucl.ac.uk
Stavroula Balabani
UCL Mechanical Engineering, University College London, London, WC1E 7JE, UK
Carolina P. Naveira-Cotta, Renato M. Cotta
Mechanical Engineering Department. - COPPE, Federal University of Rio de Janeiro, UFRJ, Brazil

Abstract. Residence time control is an important indicator of micromixer design. When using vortex shedding to enhance mixing efficiency in a micromixer, the relationship between residence time and vortex shedding becomes important; if residence time is shorter than shedding time, the fluid elements flow through the channel too quickly with no contribution of vortex shedding to mixing. Both residence time and vortex shedding depend on geometrical and flow parameters and hence in order to optimize micromixer design the effect of these parameters on mixing need to be well understood. Furthermore, the onset of vortex shedding in confined flows such as those encountered in micromixers need be elucidated. In this work, the flow field past a single cylindrical pin in a microchannel is studied experimentally using a high-speed PIV system. The effects of confinement on vortex formation are examined. Vortex shedding was observed for a channel height of two pin diameters and the shedding frequency increased with increasing lateral confinement (i.e. upon decrease in channel width at the same pin diameter). Therefore, controlling residence time via wake oscillations in pin microchannels is highly dependent on confinement.

Keywords: Micromixing, Residence time control, Vortex shedding, High speed PIV

1. INTRODUCTION

Passive micromixers rely on the microchannel geometry to mix fluids via molecular diffusion and advection. Chaotic advection is a popular mixing mechanism for the (bio)chemical and pharmaceutical industry as it significantly improves the mixing performance which is inherently low in laminar, microscale flows (Kockmann et al., 2008). Inserting obstacles, e.g. cylindrical pins or other 3D structures in a microfluidic channel can enhance mixing via chaotic advection as obstacles periodically change the direction of fluid particles, reducing the diffusion time (Nguyen and Wu, 2004). Such obstacles can also shed periodic vortices, which can further increase mixing through stretching and folding of material lines. Vortex shedding typically takes place at Reynolds number (Re) that are relatively high for microscale flows (Renfer et al., 2013a). It thus, requires high flow rates, which might reduce the residence time of the reactants and adversely affect the reactions (Lin et al., 2003). On the other hand, vortices contort flow streamlines resulting in longer residence times. This study aims to understand the relationship between average residence times and vortex formation in a single pin microchannel, and its dependence on pin diameter and confinement by microchannel walls. A high-speed micro particle image velocimetry (μPIV) method is developed to capture the vortex shedding dynamics.

2. THEORETICAL

The two non-dimensional parameters governing the vortex shedding dynamics from cylinders are Reynolds number (Re) and Strouhal number (St), defined as

$$Re = \frac{\rho U D}{\mu}, \quad St = \frac{fD}{U} \tag{1a, 1b}$$

where ρ and μ denote the fluid density and dynamic viscosity, U is the characteristic fluid velocity, D is the diameter of the cylindrical pins and f the frequency of vortex shedding.

The residence time in a micromixer can be defined as the time a reactant fluid element spends in the reactor (Fletcher, 2016). In a rectangular microfluidic channel with a single pin, to a first order of approximation, we can write the average residence time as

$$\tau_r = \frac{Reactor\ volume}{flow\ rate} = \frac{LWH}{WHU} = \frac{L}{U} = \frac{L\rho D}{Re\mu} \tag{2}$$

where τ_r is the residence time and *L, W, H* denote the length, width and height of channel, respectively, and use has been made of Eq. (1a). The time scale of vortex shedding τ_v, i.e. inverse of shedding frequency *f*, can be written as

$$\tau_v = \frac{\rho D^2}{St Re \mu}$$

(3)

Equations (2) and (3) clearly show the dependence of residence and shedding times on the channel length and the pin diameter, which offers a means to control them via the geometry. In the limiting case, if $\tau_r < \tau_v$, the fluid elements flow through the channel too quickly with no contribution of vortex shedding to mixing. The concept of residence time control via vortex shedding is illustrated in Fig. 1, where we limit ourselves to a fully laminar regime (Zdravkovich, 2007) with *Re* = 40 to 300. Figure 1a plots the variation of τ_r and τ_v with pin diameter *D* for a channel length of *L* of 1 cm, a typical length for microfluidic chips for selected Re. As expected, for each Re shown, τ_v overtakes τ_r at high enough *D*, which means that the diameter of cylindrical pin has an upper limit up to which shedding can be exploited for mixing, depending on the channel ('reactor') length. In fact, we can obtain the maximum *D* for any value of *L* by equating the expressions for τ_r and τ_v from Eqs. (2) and (3). This maximum *D* can be substituted back to Eq. (2) to obtain a relation between the maximum residence time as a function of the chip length, in the range of *Re* considered. This relation is plotted in Figure 1b. Note that from Eq. (2), τ_r reaches its maximum value at the lowest *Re* (i.e. *Re* = 40) and highest *D* ($D_{max} = St\ L$). Conversely, the lower bound can be found at high *Re* (before the flow wake becomes turbulent, *Re* = 300) and a low value of *D*, which we have assumed to be 10 μm, based on the ease of microfabrication for high aspect ratio structures. Note that the arguments presented here are not limited to single pin. For pin arrays with/without confinement from the microchannel side and top/bottom walls, the shedding frequency and range of *Re*'s changes (Renfer et al., 2013b). This will only alter the range of τ_r in Fig. 1b, which clearly offers a means to 'select' channel/pin geometry for optimal/application-specific 'choice' of residence time.
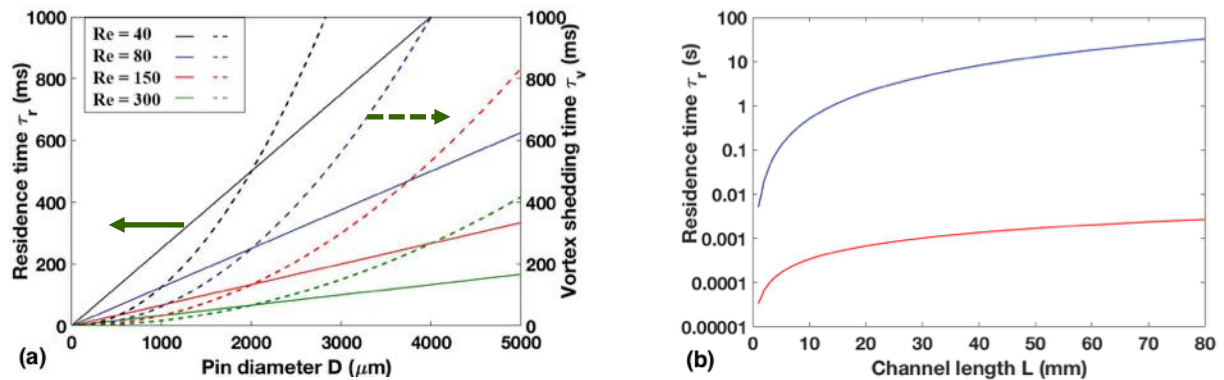

Figure 1. Geometry dependent average residence time (no confinement). (a) Variation of residence and vortex shedding times with pin diameter for a 1-cm long channel, (b) Variation in maximum and minimum residence times with channel length

3. EXPERIMENTAL SETUP

3.1. Microfluidic chip fabrication

Poly(methyl methacrylate) (PMMA) microchannels with a single cylindrical pin and different levels of vertical and lateral confinement were fabricated by CNC micro-milling (Minitech Machinery, Georgia) and bonded using an ultrasonic bonding technique (Li et al., 2008). The pin diameter was kept constant, within fabrication precision, to 600 ± 10 μm. The channel height was kept at 1,200 μm and its width varied between 1,200 - 2,400 μm, resulting in non-dimensional lateral confinement w^* (= *W / D*) ranging from 2 to 4. The total channel length was 8 cm and the distance from the inlet to the pin was 6 cm.

3.2. Methods

The experimental setup is shown schematically in Fig. 2. A custom μPIV system was assembled comprising a fiber illuminator (150 W, Thorlabs, UK), a microscope assembly (Edmund Optics, UK) and a high-speed camera (Phantom V411, USA). The microfluidic chips were mounted on an XYZ stage (Thorlabs, UK). Distilled water was used as the working fluid. The flow was seeded with 1-μm neutrally buoyant polystyrene particles (ThermoFisher, UK) and was driven by a syringe pump (Harvard Bioscience, USA) with flow rates ranging from 0.2 to 105 ml/min. The μPIV measurements were obtained in bright field mode using the polystyrene particles as tracers. 5x and 10x microscope objectives were used resulting in a spatial resolution of 4.3 μm/pixel and 1.8 μm/pixel respectively. In our setup the frame

rate ranged between 7,900 (time interval = 126 μs) and 83,000 (time interval = 12 μs) with respective maximum image sizes of 1024 × 512 pixels and 256 × 128 pixels. 5,000 images were acquired in each experiment and were processed using standard PIV algorithms. This involved a multi-pass cross-correlation procedure with a 50% overlap and starting interrogation window of 128 × 64 pixels and a final one of 32 × 32 pixels.

The 5x microscope objective was used in order to capture the wake downstream of the cylindrical pin. A flow region 6-mm (10 times than the pin diameter) upstream of the cylindrical pin was also imaged in order to determine the approaching flow velocity. The 10x microscope objective was used to capture the vortex shedding process and estimate the frequency of vortex shedding. In each case maximum possible image size was used.
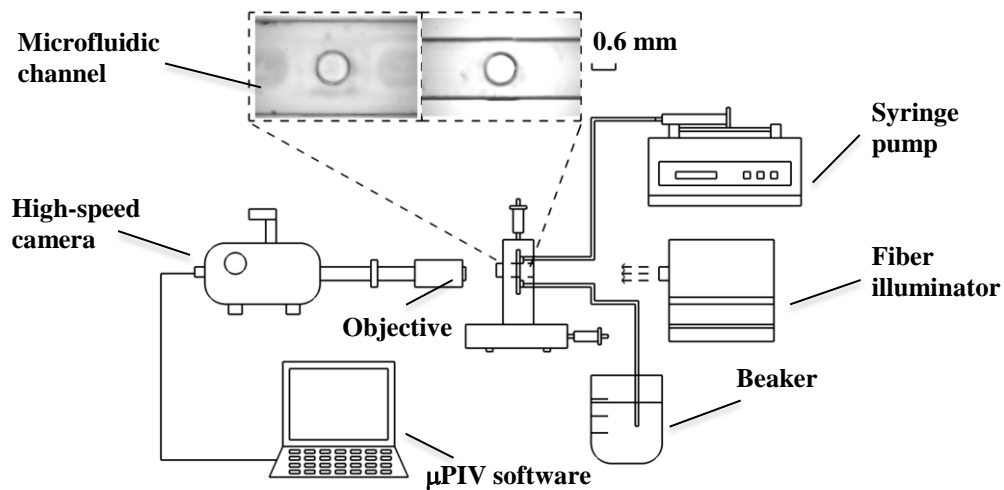

Figure 2. Schematic of the experimental setup. Insets are showing a 600 μm pin in two different microchannels, respectively, with: (a) w = 1800 μm an (b) w = 1,200 μm

4. RESULTS AND DISCUSSION

Selected instantaneous flow fields from the microfluidic chips with non-dimensional vertical confinement h^* (h/D) = 2 and lateral confinement w^* (w/D) = 3 are shown in Fig. 3. The flow fields show two elongated shear layers separating from the pin but no rolling up to form vortices. No vortex shedding was observed for Re up to 300 due to wall confinement. Evidence of some flow periodicity was firstly observed when Re reached 340; vortices appeared forming 3-3.5 diameters downstream of the pin and towards the end of the recirculation bubble (Balachandar et al., 1997). The length of the bubble reduced and vortex shedding became more apparent and stronger when Re increased to 408 or 435. The results here demonstrate that our μPIV system can capture the wake dynamics and vortex shedding processes past the micropin.
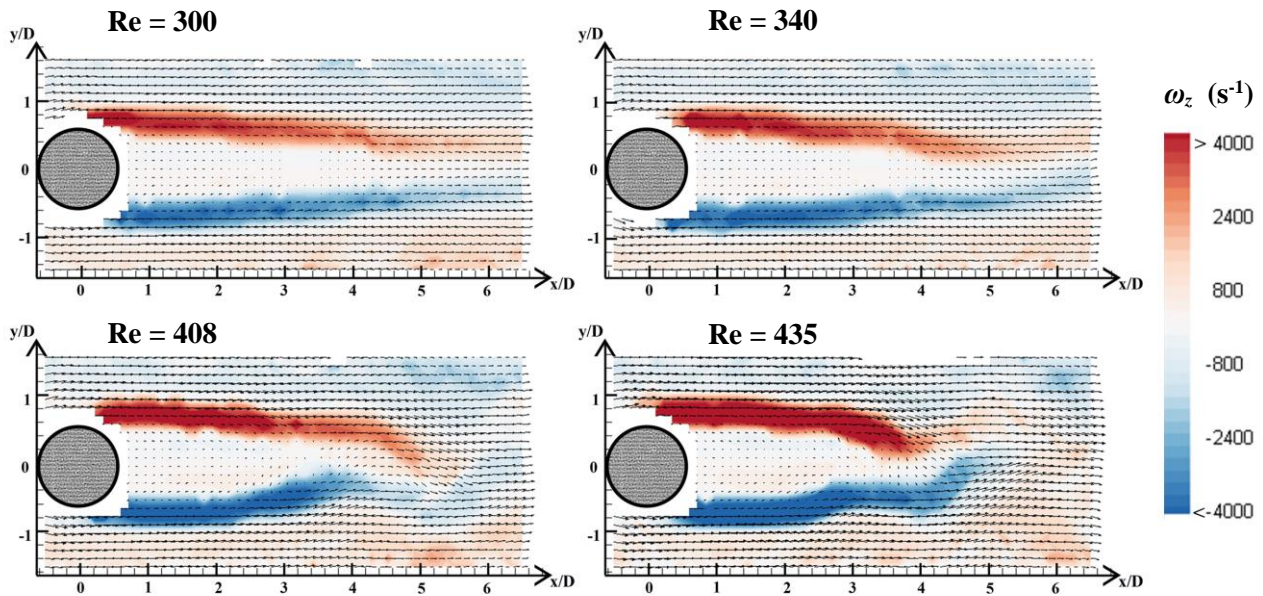
Figure 3. Instantaneous vorticity contours ω_z superimposed onto the velocity vectors for a channel with $h* = 2$ and $w* = 3$ and for different Re.

In the next set of experiments the vertical confinement was kept constant at $h* = 2$ and the lateral confinement $w*$ was varied from 2 to 4. Vector fields are not shown for brevity. However, vortex shedding was observed in all channels for Re lower than 500. In order to estimate the frequency of vortex shedding, Fast Fourier transform (FFT) was applied to the instantaneous transverse velocity signal at a selected point ($x/D = 4$, $y/D = 1$) in the wake of the pin. Figure 4a shows a typical velocity signal extracted from 5000 vector maps obtained at a framerate of 7,900 for a channel with $w* = 4$ at $Re = 322$. FFT analysis (Fig. 4b) shows a clear peak indicating a vortex shedding frequency of 258 Hz corresponding to a St of 0.231. In order to obtain more reliable results, two additional points downstream of the wake were considered ($x/D = 4$, $y/D = 0$; $x/D = 4$, $y/D = -1$) in each experiment and an average value of vortex shedding frequency was taken.
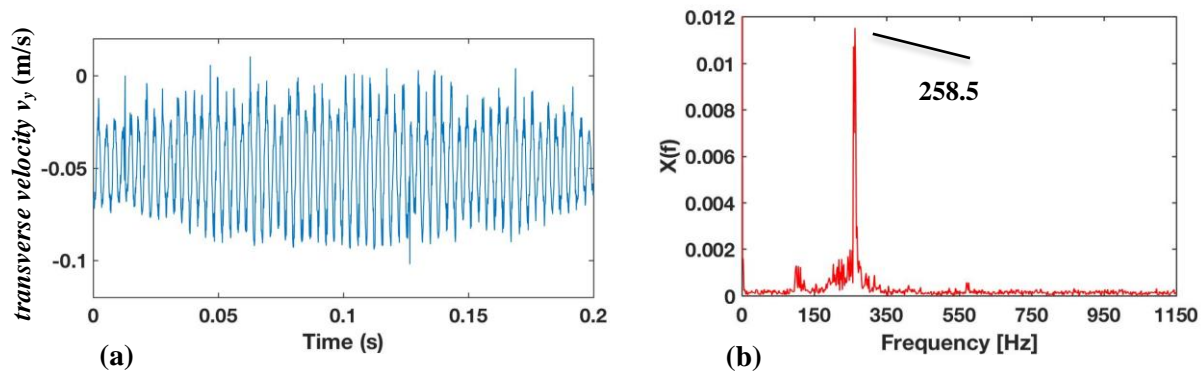

Figure 4. (a) Instantaneous transverse velocity (v) signal at a selected point in the wake, (b) Amplitude spectrum of (a) showing a distinct vortex shedding peak ($h* = 2$, $w* = 4$, Re = 322)

The estimated vortex shedding frequencies were expressed in terms of the St using eq. 1b and plotted against Re for different lateral confinements in Fig. 5. St exhibits a rising trend with increasing Re and with increasing lateral confinement (decreasing $w*$). This is in agreement with the findings of Alfieri et al. (2013) and Griffith et al. (2011). The increase in local velocities near the cylinder leads to higher shedding frequencies. Referring to Fig. 1b, the maximum τ_r depending on channel length, is related to St. Thus, the upper bound of residence time range needs to be redefined in different lateral confinement as well as different Re.
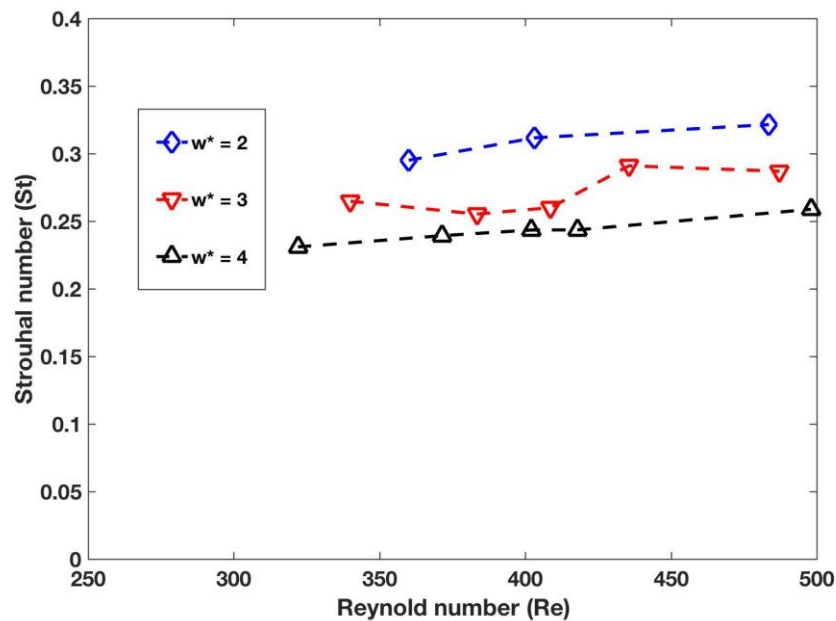
Figure 5. The relationship between *St* and *Re* in a channel with $h^* = 2$ and varying lateral confinement w^*

The lower bound of τ_r in Fig. 1b is linked to *Re* when the wake starts shedding vortices. In the channel with w* = 4, vortex shedding was first observed when *Re* reached 322. This number increased to 340 and 360 respectively in the channels with w* of 3 and 2. This implies that the sidewalls also suppress vortex shedding from the pin and delay the transition to the unsteady wake regime, in agreement with the numerical study of Singha and Sinhamahapatra (2010). Therefore, the lower bound of τ_r also needs to be redefined for different lateral confinements.

The mean axial velocity profiles measured upstream of the pin (x/D = 10) are compared in Fig. 6. The profiles are produced by averaging 1,000 images acquired at a framerate of 13,000 for a *Re* ~490. The results show that the lateral confinement results in a non-uniform flow upstream of the pin due to the boundary layers forming on the walls which can explain the *Re* differences in the onset of vortex shedding illustrated in the *St* plot (Fig. 5).
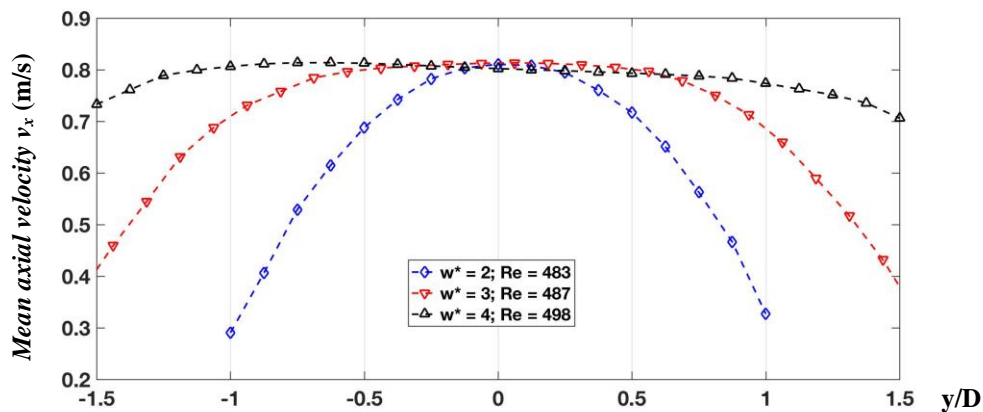

Figure 6. Axial Velocity profile upstream of the cylinder (x/D = 10) for Re around 490 with $h^* = 2$ and varying lateral confinement w^*

5. CONCLUSIONS

In this work, we proposed to exploit vortex shedding for micromixing and a geometric strategy to control the residence time to help realize continuous micromixing reaction platforms. A strategy to fully resolve the transient flow in such fluidic chips by high speed μPIV measurements in bright field mode was also introduced. The study focused on a single cylindrical pins in order to explore the role of confinement effect on the onset of vortex shedding. The confinement

suppressed/delayed shedding and affected the Strouhal number. Future work focus on understanding the relationship between confinement and residence time control for optimal mixing.

6. ACKNOWLEDGEMENTS

5. REFERENCES

Alfieri, F., Tiwari, M., Renfer, A., Brunschwiler, T., Michel, B. and Poulikakos, D. (2013). Computational modeling of vortex shedding in water cooling of 3D integrated electronics. *International Journal of Heat and Fluid Flow*, 44, pp.745-755.

Balachandar, S., Mittal, R. and Najjar, F. (1997). Properties of the mean recirculation region in the wakes of two-dimensional bluff bodies. *Journal of Fluid Mechanics*, 351, pp.167-199.

Fletcher, C. (2016). Principles of Flow Chemistry. [online] *Slideplayer.com*. Available at: http://slideplayer.com/slide/7015345/ [Accessed 21 Jan. 2017].

Griffith, M., Leontini, J., Thompson, M. and Hourigan, K. (2011). Vortex shedding and three-dimensional behaviour of flow past a cylinder confined in a channel. *Journal of Fluids and Structures*, 27(5-6), pp.855-860.

Kockmann, N., Gottsponer, M., Zimmermann, B. and Roberge, D. (2008). Enabling Continuous-Flow Chemistry in Microstructured Devices for Pharmaceutical and Fine-Chemical Production. *Chemistry - A European Journal*, 14(25), pp.7470-7477.

Li, S., Xu, J., Wang, Y., Lu, Y. and Luo, G. (2008). Low-temperature bonding of poly-(methyl methacrylate) microfluidic devices under an ultrasonic field. *Journal of Micromechanics and Microengineering*, 19(1), p.015035.

Lin, Y., Gerfen, G., Rousseau, D. and Yeh, S. (2003). Ultrafast Microfluidic Mixer and Freeze-Quenching Device. *Analytical Chemistry*, 75(20), pp.5381-5386.

Nguyen, N. and Wu, Z. (2004). Micromixers—a review. *Journal of Micromechanics and Microengineering*, 15(2), pp.R1-R16.

Renfer, A., Tiwari, M.K., Meyer, F., Brunschwiler, T., Michel, B. and Poulikakos, D. (2013a). Vortex shedding from confined micropin arrays. *Microfluidics and Nanofluidics*, 15, pp.231–242.

Renfer, A., Tiwari, M.K., Tiwari, R., Alfieri, F., Brunschwiler, T., Michel, B. and Poulikakos, D. (2013b). Microvortex-enhanced heat transfer in 3D-integrated liquid cooling of electronic chip stacks. *International Journal of Heat and Mass Transfer*, 65, pp.33–43.

Singha, S. and Sinhamahapatra, K. (2010). Flow past a circular cylinder between parallel walls at low Reynolds numbers. *Ocean Engineering*, 37(8-9), pp.757-769.

Wang, X. and Alben, S. (2015). The dynamics of vortex streets in channels. *Physics of Fluids*, 27(7), p.073603.

Zdravkovich, M. (2007). Flow around circular cylinders. 1st ed. Oxford [u.a.]: Oxford Univ. Press.